

# Constraining anomalous Higgs interactions

Tyler Corbett\*

*C.N. Yang Institute for Theoretical Physics, SUNY at Stony Brook, Stony Brook, NY 11794-3840, USA*

O. J. P. Éboli†

*Instituto de Física, Universidade de São Paulo, São Paulo – SP, Brazil. and  
Institut de Physique Théorique, CEA-Saclay Orme des Merisiers, 91191 Gif-sur-Yvette, France*

J. Gonzalez-Fraile‡

*Departament d'Estructura i Constituents de la Matèria and ICC-UB,  
Universitat de Barcelona, 647 Diagonal, E-08028 Barcelona, Spain*

M. C. Gonzalez-Garcia§

*C.N. Yang Institute for Theoretical Physics, SUNY at Stony Brook, Stony Brook, NY 11794-3840, USA  
Institució Catalana de Recerca i Estudis Avançats (ICREA), and  
Departament d'Estructura i Constituents de la Matèria,  
Universitat de Barcelona, 647 Diagonal, E-08028 Barcelona, Spain*

The recently announced Higgs discovery marks the dawn of the direct probing of the electroweak symmetry breaking sector. Sorting out the dynamics responsible for the electroweak symmetry breaking now requires probing the Higgs interactions and searching for additional states connected to this sector. In this work we analyze the constraints on Higgs couplings to the standard model gauge bosons using the available data from Tevatron and LHC. We work in a model-independent framework expressing the departure of the Higgs couplings to gauge bosons by dimension-six effective operators. This allows for independent modifications of its couplings to gluons, photons and weak gauge bosons while still preserving the SM gauge invariance. Our results indicate that best overall agreement with data is obtained if the cross section of Higgs production via gluon fusion is suppressed with respect to its Standard Model (SM) value and the Higgs branching ratio into two photons is enhanced while keeping the production and decays associated to couplings to weak gauge bosons closer to their SM value .

## I. INTRODUCTION

The electroweak symmetry breaking (EWSB) mechanism has been elusive for many decades, however the recently announced discovery of a 125 GeV Higgs boson at the CERN Large Hadron Collider (LHC) [1, 2] opens a new era in particle physics. The pressing questions now are related to the properties of this new observed state, like its spin and couplings, in order to extend our knowledge of the EWSB sector. In this work we employ the data used for the Higgs discovery to constrain its couplings to gauge bosons.

Presently there are many possible EWSB scenarios ranging from the Higgs being elementary and weakly interacting [3], as in the Standard Model , to it being composite and related to a new strongly interacting sector [4, 5]. In the last case the precision electroweak measurements and flavor changing neutral currents lead to strong constraints on strongly interacting theories, however, recent theoretical advances have made possible the construction of models in agreement with the experimental bounds [6]. The distinction between the different scenarios can be carried out by looking for further new states associated with the EWSB mechanism and/or by careful studies of the Higgs boson couplings.

In this work we assume that the observed Higgs boson is part of a  $SU(2)_L$  doublet and that possible additional states are heavy enough not to play a direct role in the low energy phenomenology. This assumption is realized in models where the Higgs boson is a pseudo-Goldstone boson of a larger broken global symmetry [7–12]. Under this assumption we consider the most general dimension-six effective lagrangian invariant under linear  $SU(3)_c \otimes SU(2)_L \otimes U(1)_Y$

---

\*Electronic address: corbett.t.s@gmail.com

†Electronic address: eboli@fma.if.usp.br

‡Electronic address: fraile@ecm.ub.es

§Electronic address: concha@insti.physics.sunysb.edu

transformations to describe the interactions of the Higgs boson with the electroweak gauge bosons, as well as with the gluons [13, 14]. For the sake of simplicity we assume that the Higgs has the same interaction with fermions as in the SM, nevertheless this hypothesis still has to be tested further<sup>1</sup>. This scenario can be falsified by the discovery of new states or by the non-observation of its predictions to the triple electroweak–gauge–boson vertices.

The effective operators describing the Higgs anomalous interactions modify both the Higgs production mechanism and its decay patterns, therefore we combine several channels to unravel the contribution of the different operators. In our analyses we use the most recent data from the Tevatron [15] and LHC at 7 TeV [16, 17] and at 8 TeV [1, 2]. Anomalous interactions also enhance the Higgs decay into  $Z\gamma$  as well as its production in association with a photon. Nevertheless, the available statistics are not enough to make these channels visible.

This work is organized as follows. In Section II we present the dimension-six effective operators and the different scenarios studied in these analyses. Details of our analyses are presented in Section III. We present our results in section IV while Section V contains our conclusions.

## II. HIGGS ANOMALOUS INTERACTIONS

In this work we assume that the Higgs boson is part of a  $SU(2)_L$  doublet, therefore we extend the SM by adding higher dimension operators that are invariant under linear  $SU(3)_c \otimes SU(2)_L \otimes U(1)_Y$  transformations. The first corrections to the Higgs couplings are expressed as dimension-six operators that can be written as

$$\mathcal{L}_{\text{eff}} = \sum_n \frac{f_n}{\Lambda^2} \mathcal{O}_n \quad , \quad (1)$$

where the operators  $\mathcal{O}_n$  involve vector–boson and/or Higgs–boson fields with couplings  $f_n$  and where  $\Lambda$  is a characteristic scale. Requiring the operators  $\mathcal{O}_n$  to be  $P$  and  $C$  even, there are only seven dimension–six operators that modify the Higgs–boson couplings to electroweak vector bosons and one to gluons [13, 14]:

$$\begin{aligned} \mathcal{O}_{GG} &= \Phi^\dagger \Phi G_{\mu\nu}^a G^{a\mu\nu} & \mathcal{O}_{WW} &= \Phi^\dagger \hat{W}_{\mu\nu} \hat{W}^{\mu\nu} \Phi \quad , & \mathcal{O}_{BB} &= \Phi^\dagger \hat{B}_{\mu\nu} \hat{B}^{\mu\nu} \Phi \quad , \\ \mathcal{O}_{BW} &= \Phi^\dagger \hat{B}_{\mu\nu} \hat{W}^{\mu\nu} \Phi \quad , & \mathcal{O}_W &= (D_\mu \Phi)^\dagger \hat{W}^{\mu\nu} (D_\nu \Phi) \quad , & \mathcal{O}_B &= (D_\mu \Phi)^\dagger \hat{B}^{\mu\nu} (D_\nu \Phi) \quad . \\ \mathcal{O}_{\Phi,1} &= (D_\mu \Phi)^\dagger \Phi^\dagger \Phi (D^\mu \Phi) \quad , & \mathcal{O}_{\Phi,2} &= \frac{1}{2} \partial^\mu (\Phi^\dagger \Phi) \partial_\mu (\Phi^\dagger \Phi) \quad , \end{aligned} \quad (2)$$

where  $\Phi$  stands for the Higgs doublet,  $D_\mu$  is the covariant derivative,  $\hat{B}_{\mu\nu} = i(g'/2)B_{\mu\nu}$ , and  $\hat{W}_{\mu\nu} = i(g/2)\sigma^a W_{\mu\nu}^a$ , with  $B_{\mu\nu}$ ,  $W_{\mu\nu}^a$ , and  $G_{\mu\nu}^a$  being respectively the  $U(1)_Y$ ,  $SU(2)_L$ , and  $SU(3)_c$  field strength tensors. We denote the  $SU(2)_L$  ( $U(1)_Y$ ) gauge coupling as  $g$  ( $g'$ ).

The effective operators in Eq. (2) give rise to anomalous  $Hgg$ ,  $H\gamma\gamma$ ,  $HZ\gamma$ ,  $HZZ$ , and  $HW^+W^-$  couplings, which in the unitary gauge are given by

$$\begin{aligned} \mathcal{L}_{\text{eff}}^{\text{HVV}} &= g_{Hgg} H G_{\mu\nu}^a G^{a\mu\nu} + g_{H\gamma\gamma} H A_{\mu\nu} A^{\mu\nu} + g_{HZ\gamma}^{(1)} A_{\mu\nu} Z^\mu \partial^\nu H + g_{HZ\gamma}^{(2)} H A_{\mu\nu} Z^{\mu\nu} \\ &+ g_{HZZ}^{(1)} Z_{\mu\nu} Z^\mu \partial^\nu H + g_{HZZ}^{(2)} H Z_{\mu\nu} Z^{\mu\nu} + h_{HZZ}^{(3)} H Z_\mu Z^\mu \\ &+ g_{HWW}^{(1)} (W_{\mu\nu}^+ W^{-\mu} \partial^\nu H + \text{h.c.}) + g_{HWW}^{(2)} H W_{\mu\nu}^+ W^{-\mu\nu} + g_{HWW}^{(3)} H W_\mu^+ W^{-\mu} \quad , \end{aligned} \quad (3)$$

where  $V_{\mu\nu} = \partial_\mu V_\nu - \partial_\nu V_\mu$  with  $V = A, Z$  and  $W$ . The effective couplings  $g_{Hgg}$ ,  $g_{H\gamma\gamma}$ ,  $g_{HZ\gamma}^{(1,2)}$ ,  $g_{HWW}^{(1,2,3)}$  and  $g_{HZZ}^{(1,2,3)}$  are

---

<sup>1</sup> The preliminary CMS [2] results indicate that the SM values for the Higgs couplings to fermions is within the 90–95% CL allowed region.

related to the coefficients of the operators appearing in (1) through,

$$\begin{aligned}
g_{Hgg} &= -\frac{\alpha_s}{8\pi} \frac{f_g v}{\Lambda^2} \\
g_{H\gamma\gamma} &= -\left(\frac{gM_W}{\Lambda^2}\right) \frac{s^2(f_{BB} + f_{WW} - f_{BW})}{2} , \\
g_{HZZ}^{(1)} &= \left(\frac{gM_W}{\Lambda^2}\right) \frac{s(f_W - f_B)}{2c} , \\
g_{HZZ}^{(2)} &= \left(\frac{gM_W}{\Lambda^2}\right) \frac{s[2s^2 f_{BB} - 2c^2 f_{WW} + (c^2 - s^2)f_{BW}]}{2c} , \\
g_{HZZ}^{(1)} &= \left(\frac{gM_W}{\Lambda^2}\right) \frac{c^2 f_W + s^2 f_B}{2c^2} , \\
g_{HZZ}^{(2)} &= -\left(\frac{gM_W}{\Lambda^2}\right) \frac{s^4 f_{BB} + c^4 f_{WW} + c^2 s^2 f_{BW}}{2c^2} , \\
g_{HZZ}^{(3)} &= \left(\frac{gM_W v^2}{\Lambda^2}\right) \frac{f_{\Phi,1} - f_{\Phi,2}}{4c^2} , \\
g_{HWW}^{(1)} &= \left(\frac{gM_W}{\Lambda^2}\right) \frac{f_W}{2} , \\
g_{HWW}^{(2)} &= -\left(\frac{gM_W}{\Lambda^2}\right) f_{WW} , \\
g_{HWW}^{(3)} &= -\left(\frac{gM_W v^2}{\Lambda^2}\right) \frac{f_{\Phi,1} + 2f_{\Phi,2}}{4} ,
\end{aligned} \tag{4}$$

where we wrote  $f_{GG} = -\frac{\alpha_s}{8\pi} f_g$  and where  $s$  and  $c$  stand for the sine and cosine of the weak mixing angle respectively. The couplings  $g_{HZZ}^{(3)}$  and  $g_{HWW}^{(3)}$  include the effects arising from the contribution of the operators  $\mathcal{O}_{\Phi,1}$  and  $\mathcal{O}_{\Phi,2}$  to the renormalization of the weak boson masses and the Higgs field wave function.

The operator  $\mathcal{O}_{BW}$  contributes at tree level to the  $W^3$ – $B$  mixing which is constrained by the electroweak precision data [18–20], therefore we do not take its effects into account in our studies. The operator  $\mathcal{O}_{\Phi,1}$  contributes to  $Z$  mass but not to the  $W$  one, therefore it is severely constrained by the  $\rho$  parameter. Moreover the operators  $\mathcal{O}_{\Phi,1}$  and  $\mathcal{O}_{\Phi,2}$  lead to a multiplicative contribution to the SM Higgs couplings to  $ZZ$  and  $WW$ . In the present analysis we do not consider the operators  $\mathcal{O}_{\Phi,1}$  and  $\mathcal{O}_{\Phi,2}$ , however their impact on the Higgs phenomenology can be seen in Refs. [2, 21–25].

In this work we focus our attention in the operators  $\mathcal{O}_{GG}$ ,  $\mathcal{O}_{BB}$ ,  $\mathcal{O}_{WW}$ ,  $\mathcal{O}_B$ , and  $\mathcal{O}_W$ . One expects the contribution of new physics to these five operators to take place at loop level [26] and consequently they are suppressed by factors  $1/(16\pi^2)$ . Therefore, we expect that the largest effect of these effective interactions should appear in the couplings of the Higgs to photon–photon and gluon–gluon since these couplings take place through loop effects in the SM.

One important property of the operators  $\mathcal{O}_B$  and  $\mathcal{O}_W$  is that they also modify the triple gauge–boson couplings  $\gamma W^+ W^-$  and  $Z W^+ W^-$ . Consequently they can be directly probed in additional channels not directly involving the Higgs boson [27–29]. The triple gauge–boson effective interaction can be rewritten in the standard parametrization of the  $C$  and  $P$  even interactions [30]:

$$\mathcal{L}_{WWV} = -ig_{WWV} \left\{ g_1^V \left( W_{\mu\nu}^+ W^{-\mu} V^\nu - W_\mu^+ V_\nu W^{-\mu\nu} \right) + \kappa_V W_\mu^+ W_\nu^- V^{\mu\nu} + \frac{\lambda_V}{m_W^2} W_{\mu\nu}^+ W^{-\nu\rho} V_\rho^\mu \right\} , \tag{5}$$

where  $g_{WW\gamma} = e$ ,  $g_{WWZ} = e/(sc)$ . In general these vertices involve six dimensionless couplings  $g_1^V$ ,  $\kappa_V$ , and  $\lambda_V$  ( $V = \gamma$  or  $Z$ ). Notwithstanding the electromagnetic gauge invariance requires that  $g_1^\gamma = 1$ , while the remaining five free couplings are related to the dimension–six operators that we are considering:

$$\begin{aligned}
\Delta g_1^Z &= g_1^Z - 1 = \frac{1}{2} \frac{m_Z^2}{\Lambda^2} f_W , \\
\Delta \kappa_\gamma &= \kappa_\gamma - 1 = \frac{1}{2} \frac{m_W^2}{\Lambda^2} (f_W + f_B) , \\
\Delta \kappa_Z &= \kappa_Z - 1 = \frac{1}{2} \frac{m_Z^2}{\Lambda^2} (c^2 f_W - s^2 f_B) , \\
\lambda_\gamma &= \lambda_Z = 0 .
\end{aligned} \tag{6}$$

In summary, in the theoretical framework that we are using the observables depend upon 5 parameters,  $f_g, f_B, f_W, f_{BB}, f_{WW}$ . In what follows for the sake of simplicity we focus on two different scenarios:

- **scenario I:** we impose that  $f_W = f_B$  and  $f_{BB} = f_{WW}$ . This scenario has three free parameters ( $f_W, f_{WW}$  and  $f_g$ ) and it exhibits a constraint between the three couplings of the Higgs to electroweak vector bosons. This scenario predicts the existence of anomalous triple electroweak gauge–boson interactions.
- **scenario II:** we set  $f_W = f_B = 0$  and  $f_{WW} = f_{BB}$ . This scenario has two free parameters ( $f_g$  and  $f_{BB} = f_{WW}$ ) and it can be considered the low–energy limit of an extension of the SM that contains an extra heavy scalar multiplet; for details see Ref. [20]. Moreover, this scenario can not be constrained by data on triple gauge–boson couplings.

The above relations (6) allow us to constrain the couplings  $f_B$  and  $f_W$  using the available experimental bounds on the effective couplings  $\Delta g_1^Z, \Delta \kappa_\gamma$  and  $\Delta \kappa_Z$  [31]. Nevertheless these experimental bounds are usually obtained assuming only one anomalous operator different from the SM value at a time, an assumption which is not consistent with our scenario I. For this reason we can not extract accurate exclusion limits from Ref. [31], but if we assume that there are no strong cancellations between the contributions of the different triple gauge–effective operators we can estimate the size of the exclusion limits on  $f_W$  and  $f_B$ . Using the 95% CL regions from Ref. [31] on  $\Delta g_1^Z, \Delta \kappa_\gamma$  or  $\Delta \kappa_Z$  we obtain that in scenario I the 95% CL regions on  $f_W = f_B$  are  $[-13, 7] \text{ TeV}^{-2}$ ,  $[-18, 9] \text{ TeV}^{-2}$  or  $[-85, 20] \text{ TeV}^{-2}$  respectively. Furthermore, the LHC collaborations are starting to look for deviations in the triple gauge–boson couplings [28, 29], however their individual limits have not reach the level of the LEP bounds yet.

### III. ANALYSES FRAMEWORK

In order to obtain the present constraints on the Higgs anomalous interactions we perform a chi-square test using the available data on the signal strength ( $\mu$ ) from Tevatron, LHC at 7 TeV and LHC at 8 TeV. We assume that the correlations between the different channels are negligible except for the theory uncertainties that are treated with the pull method [32, 33] in order to preserve the full correlation.

Schematically we can write

$$\chi^2 = \text{Min}_{\xi_{\text{pull}}} \sum_j \frac{(\mu_j - \mu_j^{\text{exp}})^2}{\sigma_j^2} + \sum_{\text{pull}} \left( \frac{\xi_{\text{pull}}}{\sigma_{\text{pull}}} \right)^2 \quad (7)$$

where  $j$  stands for channels presented in Tables I and II. We denote the theoretically expected signal as  $\mu_j$ , the observed best fitted values as  $\mu_j^{\text{exp}}$  and errors as  $\sigma_j^{+, -}$ . As we can see from these tables the errors are not symmetric, showing a deviation from a gaussian behavior as expected from the still low statistics. In our calculations we make the errors in each channel symmetric by taking

$$\sigma_j = \sqrt{\frac{(\sigma_j^+)^2 + (\sigma_j^-)^2}{2}}. \quad (8)$$

Concerning the theoretical uncertainties, the largest are associated with the gluon-gluon fusion subprocess and to account for these errors we introduce two pull factors, one for the Tevatron ( $\xi_T$ ), one for the LHC at 7 TeV and LHC at 8 TeV ( $\xi_L$ ). They modify the corresponding predictions as shown in Eqs.(12) and (13). We consider that the errors associated with the pulls are  $\sigma_L = 0.15$  and  $\sigma_T = 0.4$ . As statistics build up it will be necessary to introduce pulls associated with the theoretical uncertainties to the other production mechanisms as well as possible systematic correlated errors, however at this moment this is a sub-leading effect.

One important approximation in our analyses is that we neglect the effects associated with the distortions of the kinematical distributions of the final states due to the Higgs anomalous couplings. Thus we implicitly assume that the anomalous contributions have the same detection efficiencies as the SM Higgs. A full simulation of the anomalous operators taking advantage of their special kinematical features would increase the current sensitivity on the anomalous operators.

In order to predict the modification of the observables we need to include the effect of the anomalous operators in the production channels as well as in the decay branching ratios. As a first approximation we can assume that the  $K$  factor associated with higher order corrections is the same for the SM and anomalous contributions, so we write

$$\sigma_Y^{\text{ano}} = \frac{\sigma_Y^{\text{ano}}}{\sigma_Y^{\text{SM}}} \bigg|_{\text{tree}} \sigma_Y^{\text{SM}} \big|_{\text{soa}} \quad (9)$$

Channel	$\mu^{exp}$	comment
$p\bar{p} \rightarrow W^+W^-$	$0.32^{+1.13}_{-0.32}$	CDF & D0 [15]
$p\bar{p} \rightarrow b\bar{b}$	$1.97^{+0.74}_{-0.68}$	CDF & D0 [15]
$p\bar{p} \rightarrow \gamma\gamma$	$3.6^{+3.0}_{-2.5}$	CDF & D0 [15]
$pp \rightarrow \tau\bar{\tau}$	$0.2^{+1.7}_{-1.9}$	ATLAS [16]
$pp \rightarrow b\bar{b}$	$0.5^{+2.1}_{-2.0}$	ATLAS [16]
$pp \rightarrow ZZ^* \rightarrow \ell^+\ell^-\ell^+\ell^-$	$1.4^{+1.3}_{-0.8}$	ATLAS [16]
$pp \rightarrow WW^* \rightarrow \ell^+\nu\ell^-\bar{\nu}$	$0.5^{+0.7}_{-0.7}$	ATLAS [16]
$pp \rightarrow \gamma\gamma$	$1.6^{+0.9}_{-0.7}$	ATLAS [16]
$pp \rightarrow \tau\bar{\tau}$	$0.6^{+1.1}_{-1.2}$	CMS [17]
$pp \rightarrow b\bar{b}$	$1.2^{+2.1}_{-1.8}$	CMS [17]
$pp \rightarrow ZZ^* \rightarrow \ell^+\ell^-\ell^+\ell^-$	$0.6^{+0.9}_{-0.6}$	CMS [17]
$pp \rightarrow WW^* \rightarrow \ell^+\nu\ell^-\bar{\nu}$	$0.4^{+0.6}_{-0.6}$	CMS [17]
$pp \rightarrow \gamma\gamma$ Cat.4/BDT3	$4.1^{+4.6}_{-4.1}$	CMS [34]
$pp \rightarrow \gamma\gamma$ Cat.3/BDT2	$0.0^{+2.9}_{-0.0}$	CMS [34]
$pp \rightarrow \gamma\gamma$ Cat.2/BDT1	$2.1^{+1.5}_{-1.4}$	CMS [34]
$pp \rightarrow \gamma\gamma$ Cat.1/BDT0	$1.5^{+1.1}_{-1.0}$	CMS [34]
$pp \rightarrow \gamma\gamma jj$	$3.6^{+2.2}_{-1.6}$	CMS [34]

Table I: Processes considered in our analyses for the LHC 7 TeV run and for the Tevatron. We present the errors and best fit point for the signal strength for each topology.

Channel	$\mu^{exp}$	comment
$pp \rightarrow ZZ^* \rightarrow \ell^+\ell^-\ell^+\ell^-$	$1.3^{+0.6}_{-0.6}$	ATLAS @ 7 and 8 TeV [1]
$pp \rightarrow \gamma\gamma$	$1.5^{+0.5}_{-0.6}$	ATLAS @ 7 and 8 TeV [1]
$pp \rightarrow \tau\bar{\tau}$	$-0.18^{+0.78}_{-0.72}$	CMS @ 7 and 8 TeV [2]
$pp \rightarrow b\bar{b}$	$0.12^{+0.73}_{-0.66}$	CMS @ 7 and 8 TeV [2]
$pp \rightarrow ZZ^* \rightarrow \ell^+\ell^-\ell^+\ell^-$	$0.7^{+0.51}_{-0.35}$	CMS @ 7 and 8 TeV [2]
$pp \rightarrow WW^* \rightarrow \ell^+\nu\ell^-\bar{\nu}$	$0.6^{+0.4}_{-0.4}$	CMS @ 7 and 8 TeV [2]
$pp \rightarrow \gamma\gamma$ Untagged 3	$3.85^{+1.65}_{-1.85}$	CMS @ 8 TeV [2]
$pp \rightarrow \gamma\gamma$ Untagged 2	$1.0^{+1.05}_{-1.15}$	CMS @ 8 TeV [2]
$pp \rightarrow \gamma\gamma$ Untagged 1	$1.6^{+0.9}_{-0.9}$	CMS @ 8 TeV [2]
$pp \rightarrow \gamma\gamma$ Untagged 0	$1.9^{+1.3}_{-1.3}$	CMS @ 8 TeV [2]
$pp \rightarrow \gamma\gamma jj$ loose	$-0.6^{+2.0}_{-2.0}$	CMS @ 8 TeV [2]
$pp \rightarrow \gamma\gamma jj$ tight	$1.35^{+1.5}_{-1.5}$	CMS @ 8 TeV [2]

Table II: Available data including the 8 TeV run. We present the errors and best fit point for the signal strength for each topology.

where the ratio of the anomalous and SM cross sections of the subprocess  $Y$  ( $= gg, \text{VBF or } VH$ ) is evaluated at tree level and it is multiplied by the value for the state-of-the-art SM cross section calculations ( $\sigma_Y^{SM}|_{soa}$ ) presented in Ref. [35]. Analogously we write the decay width into the final state  $X$  as

$$\Gamma^{ano}(h \rightarrow X) = \frac{\Gamma^{ano}(h \rightarrow X)}{\Gamma^{SM}(h \rightarrow X)} \Big|_{tree} \Gamma^{SM}(h \rightarrow X) \Big|_{soa} \quad (10)$$

where the SM result  $\Gamma^{SM}(h \rightarrow X)|_{soa}$  is also obtained from Ref. [35]. The total width and branching ratios are evaluated following this recipe. We use the SM cross sections and decay widths and compute our predictions for  $m_H = 125$  GeV. The observed Higgs mass by ATLAS (126.5 GeV) [1] and CMS (125.3 GeV) are compatible within the experimental errors. We verified that the impact of changing the Higgs mass to 126.5 GeV is a sub-leading effect and does not alter our results. We did not include in our analyses an eventual invisible decay of the Higgs [36, 37], therefore the total width is obtained summing over the decays into the SM particles.

The search for Higgs decaying into  $b\bar{b}$  pairs takes place through Higgs production in association with a  $W$  or a  $Z$  so we can write

$$\mu_{b\bar{b}} = \frac{\sigma_{WH}^{ano} + \sigma_{ZH}^{ano}}{\sigma_{WH}^{SM} + \sigma_{ZH}^{SM}} \otimes \frac{\text{Br}^{ano}[h \rightarrow b\bar{b}]}{\text{Br}^{SM}[h \rightarrow b\bar{b}]} \quad (11)$$

with the superscripts  $ano$  ( $SM$ ) standing for the value of the observable considering the anomalous and SM interactions (pure SM contributions).

The channels  $\gamma\gamma jj$  take place mostly through vector boson fusion (VBF) with a 3.3% contamination coming from gluon–gluon fusion. The expected signal strength in this channel is given by

$$\mu_{jj\gamma\gamma} = \frac{0.033 \sigma_{gg}^{ano}(1 + \xi_g) + \sigma_{VBF}^{ano}}{0.033 \sigma_{gg}^{SM} + \sigma_{VBF}^{SM}} \otimes \frac{\text{Br}^{ano}[h \rightarrow \gamma\gamma]}{\text{Br}^{SM}[h \rightarrow \gamma\gamma]}. \quad (12)$$

where  $\xi_g$  is the pull associated to the gluon–gluon cross section uncertainties. The anomalous cross sections are evaluated using the prescription (9).

With the exception of the above processes, all other channels are treated as inclusive, so we write the expected signal strength of the final state  $F$  as

$$\mu_f = \frac{\sigma_{gg}^{ano}(1 + \xi_g) + \sigma_{VBF}^{ano} + \sigma_{WH}^{ano} + \sigma_{ZH}^{ano}}{\sigma_{gg}^{SM} + \sigma_{VBF}^{SM} + \sigma_{WH}^{SM} + \sigma_{ZH}^{SM}} \otimes \frac{\text{Br}^{ano}[h \rightarrow F]}{\text{Br}^{SM}[h \rightarrow F]}. \quad (13)$$

Here we also use Eqs. (9) and (10) to obtain the anomalous cross sections and branching ratios.

For some final states the available LHC 8 TeV data has been presented combined with the 7 TeV results. Given the limited available information on errors and correlations, we construct the expected theoretical signal strength as an average of the expected signal strengths for the center-of-mass energies of 7 and 8 TeV. We weight the contributions by the total number of events expected at each energy in the framework of the SM, i.e. given a final state  $X$  we evaluate

$$\mu_X^{comb} = \frac{\mu_X^{7\text{TeV}} \sigma_X^{SM,7\text{TeV}} \mathcal{L}_{7\text{TeV}} + \mu_X^{8\text{TeV}} \sigma_X^{SM,8\text{TeV}} \mathcal{L}_{8\text{TeV}}}{\sigma_X^{SM,7\text{TeV}} \mathcal{L}_{7\text{TeV}} + \sigma_X^{SM,8\text{TeV}} \mathcal{L}_{8\text{TeV}}}. \quad (14)$$

So when considering the full available data set we consider all the processes in Table I and II, neglecting the LHC 7 TeV processes whose data has been combined with the 8 TeV run; we indicate in Table II that the data has been combined by “@ 7 and 8 TeV”.

The evaluation of the relevant tree level cross section was done using the package MadGraph5 [38] with the anomalous Higgs interactions introduced using FeynRules [39]. We also cross checked our results using COMPHEP [40, 41] and VBFNLO [42]. The evaluation of the partial width was done using the expressions presented in Ref. [43].

#### IV. CONSTRAINTS ON THE HIGGS ANOMALOUS INTERACTIONS

In this section we obtain the allowed values of the Higgs interactions to vector bosons using the available Tevatron data [15], ATLAS 7 TeV [16] and 8 TeV [1] results, and CMS 7 TeV [17, 34] and 8 TeV [2] data. We find that in scenario I (II) for the global analysis  $\chi_{min}^2 = 11.9(11.9)$  for total number of 23 data points. The SM lays at  $\chi_{SM}^2 = 17.85$  or within the 89% (95%) CL region in the 3dim (2 dim) parameter space.

We present in Figure 1 the  $\Delta\chi^2$  as a function of each of the free parameters in scenario I after marginalizing with respect the other parameters. The central panel of this figure displays the  $\Delta\chi^2$  dependence on  $f_W$  for three combinations of the available data: the dotted (dashed) lines stand for the results obtained using only the LHC 7 TeV (LHC 7 TeV and Tevatron) data while the solid line is derived using the full available data set. As we can see the LHC 7 TeV data leads to a large flat region around the minimum indicating that this data set has a small sensitivity to  $f_W$ , i.e. the Higgs couplings to  $W$  and  $Z$  pairs, since the  $\gamma\gamma$  channel is the dominant one in the analysis. The addition of the Tevatron data, dominated by the Higgs associated production introduces some sensitivity to deviations in  $HZZ$  and  $HW^+W^-$ , thus in  $f_W$ , leading to the end of the flat region seen before. On the other hand, the use of the full data set drives  $f_W$  toward small values and tightens the bounds on  $f_W$ . From this panel we extract that the 95% CL  $f_W$  allowed range is  $[-13., 20.]$ .

The  $\Delta\chi^2$  dependence on  $f_{WW}$  in the scenario I is presented in the right panel of Fig. 1, where we used the same convention as in the central panel. A salient feature of this is plot is that  $\Delta\chi^2$  is concentrated around two narrow



non-overlapping regions centered around almost degenerate local minima. Notice that this degeneracy, and all others that we encounter in this work, is due to the interference between the SM and anomalous contributions. Moreover, we can see that Tevatron data has a limited impact on this parameter while the inclusion of the LHC 7 TeV results tighten the bounds on  $f_{WW}$ . From this panel we conclude that the 95% CL allowed regions are  $[-0.75, -0.04]$  and  $[1.4, 2.1]$ .

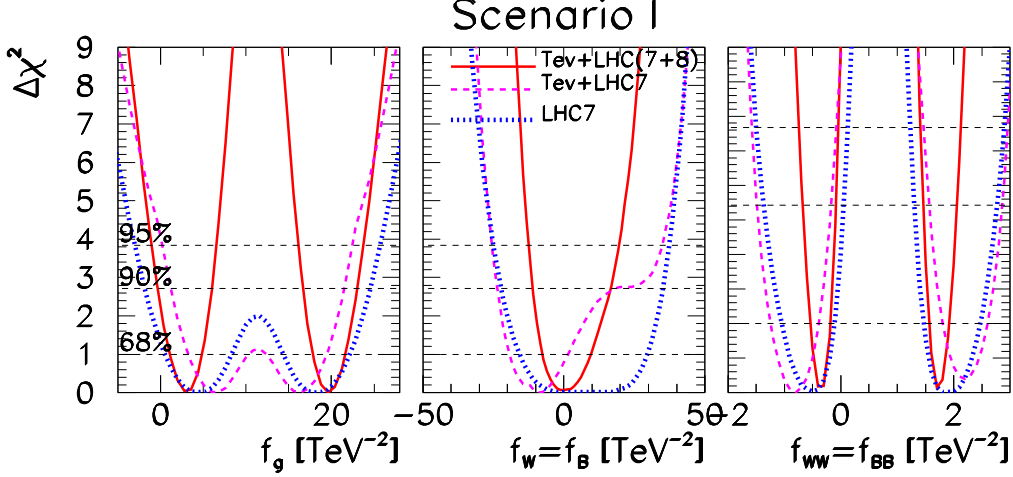


Figure 1: The left (central, right) panel exhibits  $\Delta\chi^2$  as a function of  $f_g$  ( $f_W$ ,  $f_{WW}$ ) in the framework of scenario I. Each panel contains three lines: the dotted (dashed) one was obtained using only the LHC 7 TeV (LHC 7 TeV and Tevatron) data while the solid line stands for the result using all the available data. In each panel  $\Delta\chi^2$  is marginalized over the two undisplayed parameters.

We depict the  $\Delta\chi^2$  dependence on  $f_g$  in the left panel of figure 1. In the figure not only are there almost two degenerate minima in the LHC 7 TeV result but also the 95% CL allowed region is quite large and connected. The inclusion of the Tevatron data in the analysis does not qualitatively alter the result but it helps improve the constraints. The full data set has a big impact because it leads to two non-overlapping allowed regions even at 95% CL that are  $[-1.1, 6.6]$  and  $[16., 24.]$ . The value of the gluon–fusion cross section at the minima is around 55% of its SM value and this cross section is very suppressed in the region between the minima. This very suppressed gluon–fusion cross section was not very much disfavoured before the 8 TeV data; there the CMS @ 7 TeV  $b\bar{b}$  channel allowed for a larger  $f_W$  coupling to enhance associated production, compensating consequently the very suppressed gluon–fusion cross section.

We present in Figure 2 the  $\Delta\chi^2$  dependence on  $f_{WW}$  ( $f_g$ ) using all available data. The dashed lines stand for the scenario II results while the solid line for the scenario I. The marginalization over the parameters not displayed is as explained in the figure caption. As we can see the two lines are almost coincident in both panels. This is due to the fact that in scenario I the full available data is well described by  $f_W = f_W \simeq 0$  for all allowed values of  $f_{WW}$  and  $f_g$ , consequently the two scenarios give very similar results.

Let us turn our attention towards the correlations between the three free parameters of scenario I. Figure 3 depicts 68%, 90%, 95%, and 99% CL allowed regions of the  $f_{WW} \otimes f_g$  (upper right panel),  $f_W \otimes f_g$  (upper left panel) and  $f_W \otimes f_{WW}$  (lower panel) planes using all attainable data. We obtained these plots marginalizing over the free parameter not appearing in each of the panels. We verified that the results do not change significantly when we do not employ the pulls to perform the fit. This behavior could be anticipated since the experimental errors are still much larger than the errors described by the pulls; a situation that will soon change.

We can see from the upper right panel of Fig. 3 that there are four well isolated allowed “islands” in the  $f_{WW} \otimes f_g$  plane. Moreover, within each of these islands  $f_{WW}$  and  $f_g$  are strongly correlated or anti-correlated. As mentioned before, the existence of degenerate islands is due to the interference between the SM and anomalous contributions which allow two different values of the anomalous couplings to lead to the same cross section. In the case at hand, the gluon–gluon fusion cross section preferred by the fit is around 55% of its SM value. It is interesting to notice that when we remove the  $b\bar{b}$  channel from the fit the vertical gap between two islands on the left (or on the right)

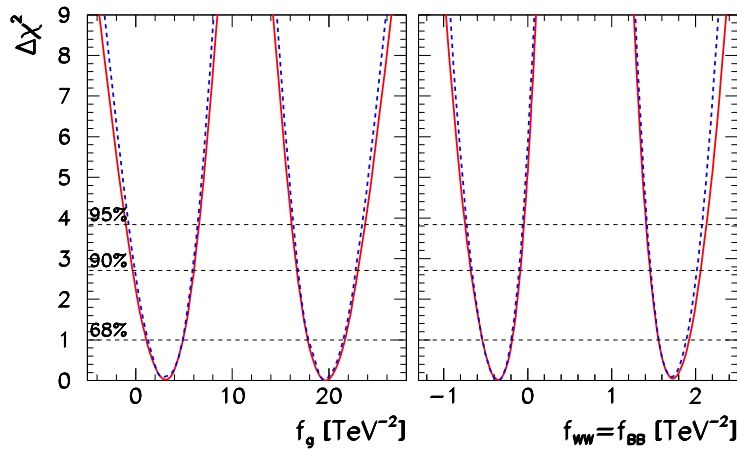


Figure 2:  $\Delta\chi^2$  as a function of  $f_g$  and  $f_{WW} = f_{BB}$  for the full combined analysis. The full lines correspond to scenario I in which  $\Delta\chi^2$  is marginalized over the two undisplayed parameters in each panel:  $f_{WW} = f_{BB}$  and  $f_W = f_B$  in the left panel, and  $f_g$  and  $f_W = f_B$  in the right panel. The dashed lines correspond to scenario II, ie imposing first the prior  $f_W = f_B = 0$  and then marginalizing over  $f_{WW} = f_{BB}$  (left) and  $f_g$  (right).

disappear. That is, intermediate values of  $f_g$  become allowed. This happens because the  $b\bar{b}$  data, which is dominated by associated production, constrains the coupling of the Higgs to  $W$  and  $Z$  pairs. In our framework, this leads to a bound on the  $H\gamma\gamma$  branching ratio. Since the  $\gamma\gamma$  data constrains the product of the gluon-gluon fusion cross section by the Higgs width into photons, the lack of a bound on the latter allows the former to have smaller values. In fact the gluon fusion cross section is further suppressed with respect to the SM value for those values of  $f_g$ . Consequently they can only become allowed at the price of an increase of  $f_B = f_W$  which enhances the VBF and associated production cross sections.

The upper left panel of figure 3 shows the presence of two isolated islands in the  $f_W \otimes f_G$  plane and that there is a correlation between the parameters within each island. Here again, the removal of the  $b\bar{b}$  data leads to the disappearance of the island between the allowed regions. The lower panel displays a behavior similar to the one observed in the central one except that it is in the  $f_W \otimes f_{WW}$  plane, obviously. The correlation in the  $f_{WW} \otimes f_g$  plane in the scenario II is almost identical to the one observed in the upper right panel of Fig. 3. As mentioned above this is due to the fact that for allowed values of  $f_{WW}$  and  $f_g$  the best fit point in scenario lies always near  $f_W = f_B \simeq 0$ .

## V. CONCLUSIONS

Once the Higgs boson like state has been discovered we must study its properties to establish if it is indeed the state predicted by the SM. In addition to that it is important to look for additional states that might play a role in the electroweak symmetry breaking. In this article we have studied the Higgs couplings to gauge bosons using a model-independent characterization of the deviations with respect to the SM values in terms of dimension-six operators. The approach still assumes that the Higgs field is a doublet of the  $SU(2)_L$  symmetry and that the deviations are due to additional new heavy states. Notwithstanding, our framework allows for independent modification of the couplings to gluons, photons and weak gauge bosons.

In doing so we have demonstrated that the present available data is enough to start gaining some information on the different Higgs coupling to gauge bosons. For instance, our analyses indicate that a reduced gluon fusion cross section is preferred when we use the full available data set. In fact, the CMS analyses [2], which uses a different framework, also points in this direction. Taking into account that the  $\gamma\gamma$  presently measured yield is above the SM prediction, the diminished gluon fusion cross section indicates an enhanced Higgs branching ratio in  $\gamma\gamma$ ; a fact observed in our analyses.

Our analyses of the scenario I shows that the presently available data prefers small values of  $f_W = f_B$ ; see figure 1 central panel. This indicates that changes to  $HZZ$  and  $HW^+W^-$ , as well as to triple gauge-boson couplings, are “small”. This behavior was expected because the data indicates that the Higgs couplings to  $W$ ’s and  $Z$ ’s agrees



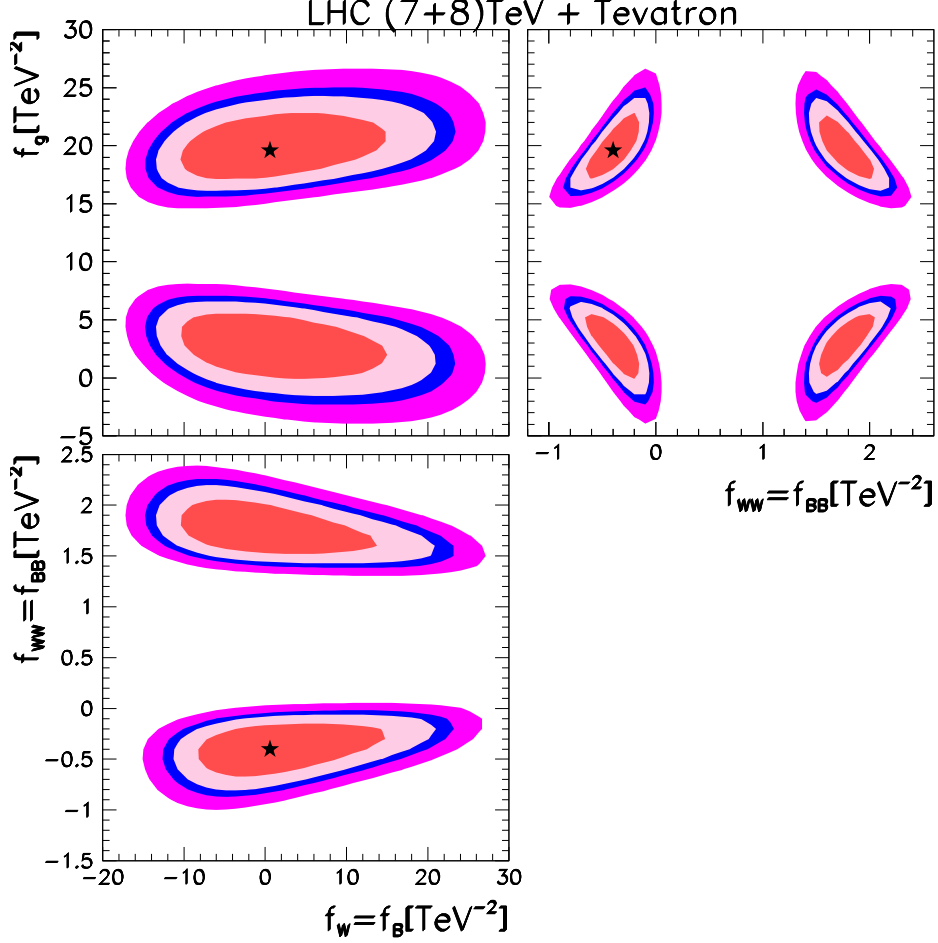


Figure 3: 68%, 90%, 95%, and 99% CL (2dof) allowed regions of the plane  $f_{WW} \otimes f_g$  (upper right panel),  $f_W \otimes f_g$  (upper left panel) and  $f_W \otimes f_{WW}$  (lower panel) using all available data. These results were obtained using the scenario I and after marginalization over the undisplayed parameter in each panel. The best fit point is indicated by a star.

with the SM within  $1\sigma$ . Furthermore, the present direct constraints on triple gauge–boson vertices lead to bounds on  $f_W$  that are of the same order as the ones derived here from Higgs phenomenology. So in the future the combined analysis of Higgs data and measurements of the anomalous triple gauge–boson couplings can be used to reduce the degeneracies observed in our results since they present a different dependence on the anomalous couplings  $f_W$  and  $f_B$ ; see Eqs. (4) and (6). In this respect, it is interesting to notice that electroweak precision measurements still give rise to the tightest limits on the Higgs anomalous interactions [20, 44].

Presently the  $\gamma\gamma$  channel is the best measured channel and its rate is above the SM prediction. The operators  $\mathcal{O}_{WW}$ ,  $\mathcal{O}_{BB}$  and  $\mathcal{O}_{GG}$  are the operators which affect this channel, therefore they are the ones showing the largest impact of the full data set. This can be seen in the strong correlations and the well isolated island present in the upper right panel of Figure 3.

We finish with a word of warning. The results presented here should be taken with a grain of salt, i.e. due to the simplifying hypothesis used in our analyses we should be aware that details can change if a more complete approach is used. Nevertheless we verified that our results are rather robust when we used only parts of the available data.

## Acknowledgments

O.J.P.E is grateful to the Institute de Physique Théorique de Saclay for its hospitality. O.J.P.E. is supported in part by Conselho Nacional de Desenvolvimento Científico e Tecnológico (CNPq) and by Fundação de Amparo à Pesquisa do Estado de São Paulo (FAPESP); M.C.G-G is also supported by USA-NSF grant PHY-0653342, by CUR Generalitat de Catalunya grant 2009SGR502 and together with J.G-F by MICINN FPA2010-20807 and consolider-ingenio 2010 program CSD-2008-0037. J.G-F is further supported by Spanish ME FPU grant AP2009-2546. T.C is supported by USA-NSF grant PHY-0653342. O.J.P.E is grateful to R. Zukanovich Funchal for enlightening discussions.

- 
- [1] ATLAS Collaboration, F. Gianotti, <http://indico.cern.ch/conferenceDisplay.py?confId=197461>.
  - [2] CMS Collaboration, I. Joseph, <http://indico.cern.ch/conferenceDisplay.py?confId=197461>.
  - [3] G. For a recent review see Altarelli, (2012), arXiv:1206.1476.
  - [4] S. Dimopoulos and L. Susskind, Nucl.Phys. **B155**, 237 (1979).
  - [5] S. Weinberg, Phys.Rev. **D19**, 1277 (1979).
  - [6] C. T. For a review see Hill and E. H. Simmons, Phys.Rept. **381**, 235 (2003), arXiv:hep-ph/0203079.
  - [7] S. Dimopoulos and J. Preskill, Nucl.Phys. **B199**, 206 (1982).
  - [8] M. J. Dugan, H. Georgi, and D. B. Kaplan, Nucl.Phys. **B254**, 299 (1985).
  - [9] D. B. Kaplan, H. Georgi, and S. Dimopoulos, Phys.Lett. **B136**, 187 (1984).
  - [10] H. Georgi, D. B. Kaplan, and P. Galison, Phys.Lett. **B143**, 152 (1984).
  - [11] G. Giudice, C. Grojean, A. Pomarol, and R. Rattazzi, JHEP **0706**, 045 (2007), arXiv:hep-ph/0703164.
  - [12] K. Agashe, R. Contino, and A. Pomarol, Nucl.Phys. **B719**, 165 (2005), arXiv:hep-ph/0412089.
  - [13] W. Buchmuller and D. Wyler, Nucl.Phys. **B268**, 621 (1986).
  - [14] C. N. Leung, S. Love, and S. Rao, Z.Phys. **C31**, 433 (1986).
  - [15] The CDF Collaboration, the D0 Collaboration, Higgs Working Group, t. T. N. Physics, (2012), arXiv:1207.0449.
  - [16] ATLAS Collaboration, G. Aad *et al.*, (2012), arXiv:1207.0319.
  - [17] CMS Collaboration, S. Chatrchyan *et al.*, Phys.Lett. **B710**, 26 (2012), arXiv:1202.1488.
  - [18] K. Hagiwara, S. Ishihara, R. Szalapski, and D. Zeppenfeld, Phys.Rev. **D48**, 2182 (1993).
  - [19] K. Hagiwara, R. Szalapski, and D. Zeppenfeld, Phys.Lett. **B318**, 155 (1993), arXiv:hep-ph/9308347.
  - [20] S. Alam, S. Dawson, and R. Szalapski, Phys.Rev. **D57**, 1577 (1998), arXiv:hep-ph/9706542.
  - [21] J. Espinosa, C. Grojean, M. Muhlleitner, and M. Trott, JHEP **1205**, 097 (2012), arXiv:1202.3697.
  - [22] J. Ellis and T. You, (2012), arXiv:1204.0464.
  - [23] D. Carmi, A. Falkowski, E. Kuflik, and T. Volansky, (2012), arXiv:1202.3144.
  - [24] A. Azatov, R. Contino, and J. Galloway, JHEP **1204**, 127 (2012), arXiv:1202.3415.
  - [25] M. Klute, R. Lafaye, T. Plehn, M. Rauch, and D. Zerwas, (2012), arXiv:1205.2699.
  - [26] C. Arzt, M. Einhorn, and J. Wudka, Nucl.Phys. **B433**, 41 (1995), arXiv:hep-ph/9405214.
  - [27] O. J. Eboli, M. Gonzalez-Garcia, S. . Lietti, and S. Novaes, Phys.Lett. **B478**, 199 (2000), arXiv:hep-ph/0001030.
  - [28] ATLAS Collaboration, G. Aad *et al.*, (2012), arXiv:1205.2531.
  - [29] CMS collaboration, A. Martelli and f. t. C. collaboration, (2012), arXiv:1201.4596.
  - [30] K. Hagiwara, R. Peccei, D. Zeppenfeld, and K. Hikasa, Nucl.Phys. **B282**, 253 (1987).
  - [31] Particle Data Group, K. Nakamura *et al.*, J.Phys.G **G37**, 075021 (2010).
  - [32] G. Fogli, E. Lisi, A. Marrone, D. Montanino, and A. Palazzo, Phys.Rev. **D66**, 053010 (2002), arXiv:hep-ph/0206162.
  - [33] M. Gonzalez-Garcia and M. Maltoni, Phys.Rept. **460**, 1 (2008), arXiv:0704.1800.
  - [34] CMS Collaboration, S. Chatrchyan *et al.*, Phys.Lett. **B710**, 403 (2012), arXiv:1202.1487.
  - [35] LHC Higgs Cross Section Working Group, S. Dittmaier *et al.*, (2011), arXiv:1101.0593.
  - [36] J. R. Espinosa, M. Muhlleitner, C. Grojean, and M. Trott, (2012), arXiv:1205.6790.
  - [37] M. Raidal and A. Strumia, Phys.Rev. **D84**, 077701 (2011), arXiv:1108.4903.
  - [38] J. Alwall, M. Herquet, F. Maltoni, O. Mattelaer, and T. Stelzer, JHEP **1106**, 128 (2011), arXiv:1106.0522.
  - [39] N. D. Christensen and C. Duhr, Comput.Phys.Commun. **180**, 1614 (2009), arXiv:0806.4194.
  - [40] A. Pukhov *et al.*, (1999), arXiv:hep-ph/9908288.
  - [41] CompHEP Collaboration, E. Boos *et al.*, Nucl.Instrum.Meth. **A534**, 250 (2004), arXiv:hep-ph/0403113.
  - [42] K. Arnold *et al.*, (2011), arXiv:1107.4038.
  - [43] M. Gonzalez-Garcia, Int.J.Mod.Phys. **A14**, 3121 (1999), arXiv:hep-ph/9902321.
  - [44] K. Hagiwara, S. Matsumoto, and R. Szalapski, Phys.Lett. **B357**, 411 (1995), arXiv:hep-ph/9505322.